4-1-2021

On the Stability of Neon Cluster Ions – Evidence for Isomeric Structures

Siegfried Kollotzek
University of Innsbruck

Stefan Bergmeister
Universität Innsbruck

Lukas Tiefenthaler
University of Innsbruck

Simon Albertini
University of Innsbruck

Elisabeth Gruber
University of Innsbruck

See next page for additional authors

Recommended Citation

S. Kollotzek, S. Bergmeister, L. Tiefenthaler, S.Albertini, E. Gruber, F. Zappa, P. Scheier, O. Echt, On the Stability of Neon Cluster Ions – Evidence for Isomeric Structures, Int. J. Mass Spectrom. 462 (2021) 116528, DOI: 10.1016/j.ijms.2021.116528, Feb 2021.

International Journal of Mass Spectrometry 462 (2021) 116528

Contents lists available at ScienceDirect

International Journal of Mass Spectrometry

journal homepage: www.elsevier.com/locate/ijms

On the stability of neon cluster ions – Evidence for isomeric structures

Siegfried Kollotzek [a], Stefan Bergmeister [a], Lukas Tiefenthaler [a], Simon Albertini [a], Elisabeth Gruber [a], Fabio Zappa [a], Paul Scheier [a, **], Olof Echt [a, b, *]

[a] Institut für Ionenphysik und Angewandte Physik, Universität Innsbruck, A-6020, Innsbruck, Austria
[b] Department of Physics, University of New Hampshire, Durham, NH, 03824, USA

ARTICLE INFO

Article history:
Received 16 November 2020
Received in revised form
14 January 2021
Accepted 16 January 2021
Available online 23 January 2021

Keywords:
Helium nanodroplets
Neon clusters
Cations
Magic numbers
Stability
Evaporation

ABSTRACT

We have adopted the newly developed technique of growing cationic clusters in size-to-charge selected helium nanodroplets (HNDs), with subsequent removal of helium in a collision cell, to record high-resolution mass spectra of Ne_n^+. Growth in singly charged HNDs leads to mass spectra that feature the same anomalies in the cluster ion abundance as in previous work, namely maxima at $n = 14$, 21, 55/56, 75. Several other, weaker but statistically significant anomalies are observed at $n = 9$, 26, 29, 33, 35, 69, 82, 89. However, when neon clusters are grown in larger HNDs, which are likely to be multiply charged, we observe a different set of magic numbers, at $n = 7$, 13, 19, 26, 29, 34, 55, 71, 81, plus many other numbers for larger clusters, up to $n = 197$. A transition from the first to the second set is observed in a limited size range if the collision pressure is increased. The most likely reason for the existence of two different sets of magic numbers appears to be the existence of two distinct structural families.

1. Introduction

The arrangement of atoms in a small atomic cluster X_n rarely resembles that in bulk matter. Small is different. However, it is difficult to calculate the energetically most stable structure of a cluster containing more than a handful of atoms. It is equally difficult to measure the actual structure of a cluster, or cluster ion, in an experiment.

Theorists face numerous challenges. First, the energy landscapes of clusters are extremely complex [1]. A cluster as small as X_{13} has no less than 988 distinct, stable minima if the interaction between the building blocks is described by the Lennard-Jones potential [2]. The number of local minima increases exponentially with increasing size n; a systematic search for the global energy minimum rapidly becomes prohibitive. The number of local minima decreases for softer potentials, but the minimum-energy structure for, say, a Morse potential may differ from that for a Lennard-Jones potential [2]. Second, pairwise additive potentials cannot accurately account for the interaction. Even in clusters of the heavy noble gases (neon through xenon), three-body contributions are not negligible [3–5]. Third, nuclear quantum effects cannot be neglected either [6,7].

Fourth, most experimental data pertain to charged clusters whose theoretical description is even more challenging. In homonuclear noble gas clusters the positive charge is partly delocalized. The dimer ion of, e.g., neon is bound by 1.28 eV [8]. In clusters the charge spreads over two, three or perhaps even four atoms. Details differ between the noble gases. For neon the ionic core probably consists of Ne_3^+ in $D_{\infty h}$ symmetry; the computed $Ne–Ne_2^+$ binding energy is 0.10 eV [8]. In mid-sized argon and xenon clusters the charge may spread over four atoms [9], but for even bigger xenon clusters the ionic core seems to shrink back to the trimer and eventually the dimer [10]. The trimer and tetrameric cores exist in linear and non-linear isomers [11,12]. Even small changes in the structure of the ionic core may lead to profound differences in the structures of clusters [13].

Experimentalists have few structural tools at their disposal that can be applied to clusters that are not supported [14]. Electron diffraction by neutral clusters averages over large size ranges [15,16]. Electron diffraction of charged, size-selected clusters is a powerful tool [17] but it has not yet been applied to weakly bound cluster ions. Most spectroscopic methods are unsuited for clusters containing several atoms except perhaps for infrared absorption

* Corresponding author. Institut für Ionenphysik und Angewandte Physik, Universität Innsbruck, A-6020, Innsbruck, Austria.
** Corresponding author.
E-mail addresses: paul.scheier@uibk.ac.at (P. Scheier), olof.echt@unh.edu (O. Echt).

https://doi.org/10.1016/j.ijms.2021.116528

spectra which has provided structural information for select systems [18,19], and for measurements of matrix shifts by messenger spectroscopy that have provided information about solvation shells [20–23].

In the present work we resort to the proven technique of identifying local anomalies (or magic numbers) in the abundance distribution of cluster ions. The method rests on the strong dependence of the evaporation rate on the evaporation energy. The relative abundances in an ensemble of initially excited clusters will reflect their relative stabilities if the clusters form an "evaporative ensemble," i.e. all clusters are smaller than they once were [24]. The assumption applies to typical ensembles of cluster ions interrogated by mass spectrometry. However, the exact relation between energies and abundances is difficult to quantify [25–27]. First, properties other than stability, including entropy and heat capacity, will play a role as well [27–29]. Second, the (charged) clusters need time to cool down and solidify into ordered structures with size-dependent stabilities before the ensemble can develop abundance anomalies [30–35]. Third, for long times the contrast in the abundance distributions will decrease again [24,35]. Fourth, a mass spectrometer does not simply provide a "snapshot" of the abundance distribution at a specific time. Depending on the type of instrument, fragment ions produced by unimolecular dissociation will contribute to the precursor ion signal, the fragment ion signal, or be rejected entirely [36,37].

In short, although the contrast in abundance distributions depends on several factors [38], the appearance of magic numbers provides valuable information. They have helped to identify the occurrence of complete-shell Mackay icosahedra in large noble gas cluster ions [39–45], rock-salt structure in metal halides [46,47], and the cage-like icosahedral structure of C_{60} [48].

Irrespective of details, a local maximum in the abundance I_n of clusters (or cluster ions) X_n, or a large abundance ratio I_n/I_{n+1} is commonly viewed as indicating a relatively high evaporation energy D_n of X_n, and/or a relatively low evaporation energy D_{n+1}. The magic numbers are robust; small differences in magic numbers reported for a specific system by ±1 mostly arise from applying different criteria for their selection. Thus, magic numbers in the abundance distribution provide a fingerprint which may help to confirm or reject the stability pattern derived from a structural model [49,50].

Argon clusters were among the first systems for which mass spectra were reported beyond size $n \approx 10$. A steep drop in the abundance after Ar_{14}^+ and a local minimum at Ar_{20}^+ were observed [51]. The authors did acknowledge a possible relation to cluster stability, but their main interest was in nucleation phenomena. An extended series of magic numbers was then noted in spectra of xenon clusters [39]. Particularly prominent ones, at $n = 13$, 55, 147, agreed with the number of atoms required to form complete-shell Mackay icosahedra. Several other anomalies were consistent with the expected closure of subshells [52], and evaporation energies calculated for neutral noble gas clusters [53].

Since then, several groups have reported mass spectra of argon [29,40,42,44,51,54–60], krypton [43,44,54,56,61–63], and xenon clusters [29,44,56,64], formed by a variety of methods. One overarching conclusion from these data is that argon, krypton, and xenon have different fingerprints, although for very large clusters, beyond $n \approx 147$ where the third Mackay icosahedron is formed, the fingerprints become similar.

Neon has received much less attention. Among previous reports [41,63,65,66], only one covers sizes at and above the second icosahedral shell closure [41]. The largest cluster detected in that work was Ne_{90}^+. In the present work we present high-resolution mass spectra of Ne_n^+ containing up to 280 atoms. Previously reported magic numbers (most prominently at $n = 14$, 21, 56, and 75) are reproduced if neon clusters are grown in singly charged HNDs. However, growth in larger, multiply charged HNDs leads to a different set of magic numbers, including at $n = 13$, 19, 55, 71, and 81. Several magic numbers are identified at and above $n = 109$, up to 197; they agree surprisingly well with previously reported numbers for heavier noble gases. The two different sets of magic numbers suggest that two distinct structural families exist that do not interconvert when the cluster ions are excited in collisions with a thermal gas of helium.

2. Experiment

In the present work we adopt a novel method to form neon cluster ions, namely by doping charged, size-selected HNDs. A diagram of the apparatus has been published elsewhere [67]. Two slightly different instruments have been used to record data which will be referred to as set 1 and 2, respectively. HNDs are formed by supersonic expansion of pre-cooled helium (Linde, purity 99.9999 %) through a nozzle (5.7 μm diameter, stagnation pressure 20 and 28 bar for set 1 and 2, respectively, temperature 9.7 and 9.8 K) into vacuum. The expanding beam is skimmed by a conical skimmer (Beam Dynamics). The size distribution of the HNDs will be broad but their speed distribution is narrow. Therefore, their kinetic energy is proportional to their size N.

The beam of HNDs is crossed by a beam of electrons (energy 70 and 38 eV, respectively, emission current 630 and 470 μA). Multiple collisions with electrons may result in highly charged HNDs [68]. The He_N^{z+} ions are accelerated into an electrostatic deflector. Ions that are transmitted have a specific mass-to-charge ratio m/z, hence a specific size-to-charge ratio N/z. However, the Rayleigh instability limits their maximum charge state z_{max}, depending on the value of N [69]. Data sets 1 and 2 were recorded with the deflector being tuned to $N/z = 4.67 \times 10^4$ and 1.9×10^5, respectively, corresponding to $z_{max} = 1$ and 28, respectively [68].

The N/z selected HNDs pass through a pickup cell (length 5.0 and 13.4 cm, respectively) filled with neon gas at ambient temperature. The pressures, measured with a cold cathode ionization gauge (Pfeiffer model IKR 251), were 0.029 Pa and 0.007 Pa, respectively (all pressures given here are corrected for the sensitivity of the ion gauge which is specified as 0.24 for neon and 0.17 for helium). Collisions between the charged HNDs and neon will lead to capture of Ne atoms, growth of Ne_n^+ in the droplet, and evaporation of helium atoms from the droplet (which, in turn, may trigger fission, see below). In a multiply charged HND, z singly charged Ne_n^+ will form. They will reside near the surface of the droplet because of the mutual Coulomb repulsion. We assume that the z embedded clusters are approximately equally sized because cluster growth is a statistical process. However, there may be factors that invalidate this assumption. In particular, a large cluster may grow at a larger rate because its capture cross section and its polarizability, hence its interaction with a freshly captured Ne atom, are larger than that of a small cluster. A failure of our assumption would affect details in our discussion in Section 4.3, but the assumption is by no means essential.

The doped HNDs that exit the pickup cell pass through three regions in which they are guided by a radio frequency (RF) field. The components are taken from a commercial Quadrupole TOF (Q-TOF) mass spectrometer (Q-TOF Ultima from Micromass, Waters). The first one, a RF hexapole (length $L = 26$ cm), contains helium gas at ambient temperature. This cell will be referred to as evaporation cell; collisions between the gas and the doped HNDs will lead to evaporation of the helium.

Multiply charged HNDs will undergo spontaneous fission if N falls below the corresponding size limit N_z. Experiments with undoped droplets have shown that fission produces a very small,

singly charged HND plus a large droplet that carries nearly all of the He atoms and z-1 charges [68]. A doped, z-fold charged HND that evaporates He atoms will eventually undergo fission into one nearly bare Ne_n^+ plus a large, doped HND that contains z-1 singly charged neon clusters.

Fission may already happen in the pickup cell if the initial charge z is close to z_{max}. In that case, the z-1 neon cluster ions embedded in the large fission fragment will keep growing until another fission event happens, producing a HND with z-2 embedded cluster ions that keep growing [70]. Eventually, a HND containing z-x singly charged Ne_n^+ (with $0 \leq x < z$) will exit the pickup cell and enter the evaporation cell where it will continue to shrink and fission until it reaches the size limit of a doubly charged droplet, $N_2 = 50\,000$, and fissions one last time into a nearly bare Ne_n^+ plus $He_{\approx 50000}Ne_n^+$. In the discussion we will refer to the latter ion as "sole survivor."

The ions that exit the evaporation cell are extracted into a commercial time-of-flight mass spectrometer equipped with a double reflectron in W configuration and a microchannel plate (MCP) detector (Micromass Q-TOF Ultima mass spectrometer, Waters). The mass resolution was 8000 and 21000 (measured at full-width-half-maximum, FWHM) for data sets 1 and 2, respectively.

Mass spectra were evaluated by means of a custom-designed software that corrects for experimental artifacts such as background signal levels, non-gaussian peak shapes, and mass drift over time [71]. The routine takes into account the isotope pattern of all ions that might contribute to a specific mass peak in order to retrieve the abundance of ions with a specific stoichiometry.

3. Results

Fig. 1 displays four mass spectra that were recorded with identical settings in the HND source, electron ionizer, electrostatic deflector, and pickup cell. These spectra are members of data set 1; experimental parameters are specified in Section 2. The pressure P_{He} in the helium evaporation cell was increased from 0.069 Pa in panel a to 0.198 Pa in panel d.

The size distributions of the observed Ne_n^+ cluster ions are bell-shaped because they are grown in singly charged, mono-disperse HNDs (the deflector was tuned to pass HNDs with a size-to-charge ratio $N/z = 4.67 \times 10^4$ which restricts the charge state to $z = 1$ [68]). When the doped HNDs enter the collision cell they will first shed their remaining helium atoms, and then neon atoms. The collision pressure in Fig. 1a was deliberately chosen to evaporate nearly all the He atoms but barely any Ne atoms. As the collision pressure is increased (Fig. 1b through 1d), the size distribution of Ne_n^+ shifts to the left.

Several anomalies are readily seen in the mass spectra. Most pronounced is the previously reported [33,41] feature in the vicinity of $n = 55$ where the second shell of the Mackay icosahedron closes. The peak at $n = 55$ forms a local maximum and the peak at $n = 56$ is followed by another steep drop; we will denote this anomaly as 55/56. Other prominent features, namely maxima at $n = 14$ and 21, and a steep drop after 75, have been noted before [33,41,63,65]. A few other local anomalies, e.g. at $n = 9$, 29, 35, 82, are also obvious if one applies either one of the following two criteria: a singular maximum, or a particularly steep drop in the peak height.

Steep drops or local maxima are difficult to spot in regions where the peak height is rapidly increasing or decreasing *versus* size. The task of identifying magic numbers is less ambiguous if the effect of the overall distribution, or its "envelope", is removed. There are several possible approaches, e.g. taking the logarithmic difference of peak amplitudes [72], subtracting the envelope from the spectrum [45,73], or dividing by the envelope [29]. We choose to first determine the ion abundance of Ne_n^+ by integrating the ion yield over all its isotopologues (which are fully resolved, see the inset in Fig. 1c). The abundance is then divided by the local average of the abundances between sizes $n - 4$ and $n + 4$ to obtain the *relative* abundance.

The size dependence of the relative abundance, extracted from the mass spectra in Fig. 1, is displayed in Fig. 2. The four data sets are stacked, the average value for each set equals 1 by definition. The top trace reveals prominent magic numbers at $n = 55/56$ and 75, and weaker ones at $n = 69$, 82, 89. These magic numbers become more prominent in spectra recorded with $P_{He} = 0.129$ Pa. Several other magic numbers appear below $n = 55$; they become even more prominent in the 3rd and 4th trace.

The contrast in the relative abundance can be read from the ordinate where the minor tick marks are spaced by 0.5. For example, in the 3rd trace ($P_{He} = 0.153$ Pa) the relative abundance of Ne_n^+ drops from 1.4 to 0.7 between $n = 14$ and 15. The magic numbers in Fig. 2 indicate those sizes for which I_n/I_{n+1} forms a statistically significant local maximum (the statistical error bars of the data in Fig. 2 are smaller than the symbol size).

The size of Ne_n^+ clusters grown in HNDs with $N/z = 4.67 \times 10^4$ (data set 1) is limited to $n \approx 100$ [67]. Growth of larger Ne clusters requires larger values of N/z, with the consequence that z is no longer limited to 1. In Fig. 3 we present mass spectra of Ne clusters grown in HNDs with $N/z = 1.9 \times 10^5$ whose maximum charge state equals $z_{max} = 28$ (data set 2). The collision pressure P_{He} was increased from 0.100 Pa to 0.117 Pa to 0.149 Pa (panels c through a). For reference, we also list the spectra IDs (ID35, ID34, and ID32, respectively). Prominent magic numbers are indicated. The largest magic number that can be clearly identified in panel b is $n = 197$.

Even larger magic numbers are apparent in panel c, but determining their exact values is impossible for two reasons: First, the statistical noise is large. Second, beyond $n \approx 200$ the conversion from mass to cluster size becomes increasingly imprecise. Neon has three naturally occurring isotopes: ^{20}Ne (mass 19.99244 u, natural abundance 90.48 %), ^{21}Ne (20.99385 u, 0.27 %), and ^{22}Ne (21.99139 u, 9.25 %), but the isotope abundance in clusters may be different [67]. This difference poses no problems for small clusters because the distributions of isotopologues for clusters of adjacent sizes are well separated, as illustrated in the inset in Fig. 1c. For large clusters, however, the distributions overlap as illustrated in the inset in Fig. 3b. We cannot resolve nominally isobaric isotopologues that belong to adjacent cluster sizes (the mass difference between ten ^{22}Ne and eleven ^{20}Ne is only 0.003 u). At $n \approx 148$ we can still determine the cluster size by counting the maxima in the envelope of the mass spectrum; that approach fails beyond $n \approx 200$ when the FWHM of the distribution of isotopologues exceeds the mass of ^{20}Ne.

The relative abundances are summarized in Fig. 4. The top trace in Fig. 4a represents the average of 12 data sets (compiled in Fig. S1 of the Supplemental Information) that were recorded with singly charged HNDs; the magic numbers are those that were indicated in Figs. 1 and 2. Data in the other 3 traces are extracted from the mass spectra in Fig. 3. Vertical lines flag anomalies that are most prominent in the bottom trace. Below $n \approx 100$ there are striking differences between the traces. First, magic numbers in set 1, at $n = 9$, 14, 21, 26, 29, 33, 35, differ from those in set 2 which occur at $n = 7$, 13, 19, 26, 29, 34. Second, the numbers change from $n = 69$, 75, 82 in the top trace to 71, 81 in the bottom trace. A transition appears to occur between the 2nd and 3rd trace as the collision pressure is changed. Also note the change from the "mixed" anomaly at 55/56 in the top trace to a distinct feature at 55 in the bottom trace.

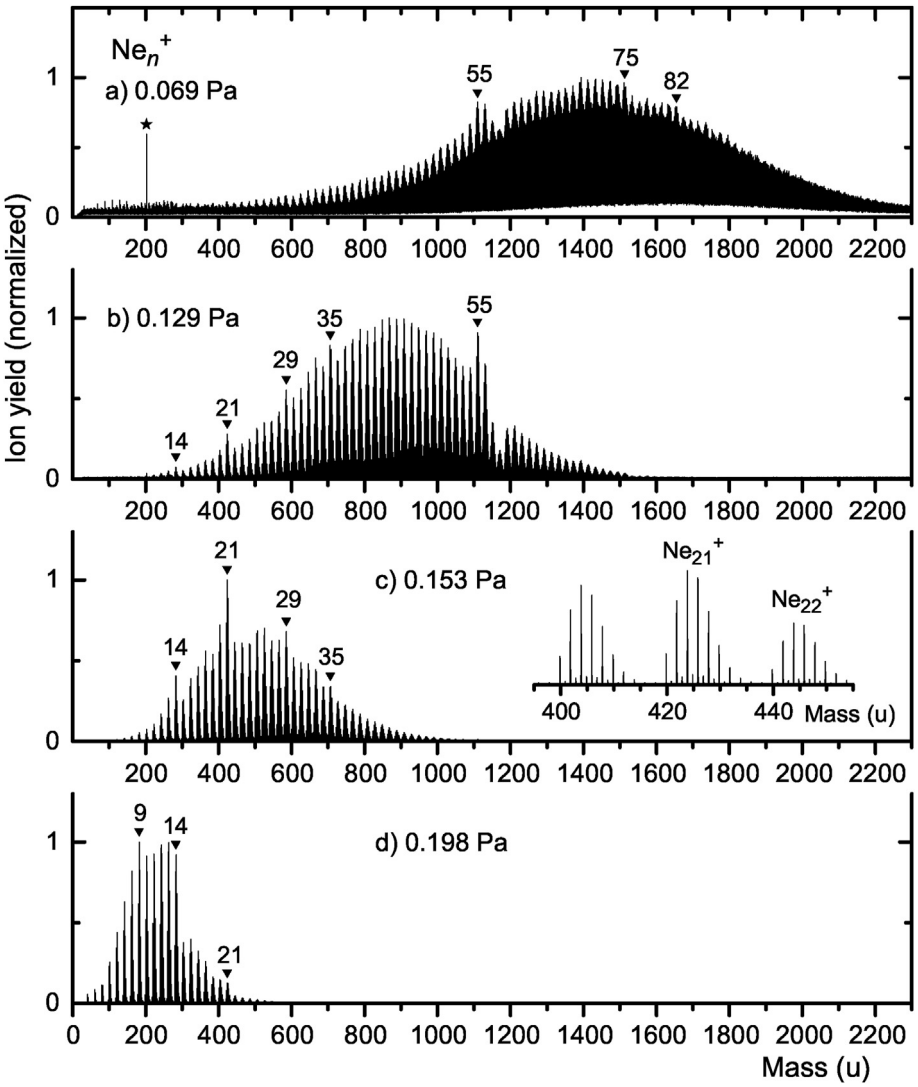

Fig. 1. Four mass spectra of neon clusters grown in singly charged HNDs (date set 1), recorded with different pressures in the evaporation cell where the doped HNDs are stripped of the helium. The bare neon cluster ions shrink as the pressure P_{He} is increased from 0.069 Pa (panel a) to 0.198 Pa (panel d). Prominent local anomalies in the ion yield *versus* size n are indicated. The asterisk in panel a flags an impurity. The expanded section of the mass spectrum in panel c reveals the isotopologues of Ne_n^+ for $n = 20, 21, 22$.

4. Discussion

We have used a novel approach to produce neon cluster ions, namely by passing pre-ionized, size-to-charge selected HNDs through a pickup cell. Excess helium atoms, and some neon atoms, are then evaporated in a separate evaporation cell by gentle collisions with helium gas at ambient temperature. Data in set 1 (displayed in Figs. 1, 2, and S1 of the Supplemental Information) were obtained by doping singly charged HNDs. They feature prominent magic numbers at 14, 21, 55/56, 75, and less pronounced but statistically significant magic numbers at 9, 26, 29, 33, 35, 69, 82, 89. Data obtained by averaging over 12 spectra are presented in the top trace in Fig. 4a. The anomalies are immune to changes in the pressure in the He evaporation cell.

The experimental approach avoids the large amount of excitation energy that is released when neutral neon clusters (either bare or embedded in helium) are ionized. To be clear, the total amount of energy release will be comparable in the two approaches, but in the present approach, energy is released primarily upon charge transfer to the first incoming Ne atom, and formation of Ne_2^+. The energy released later, upon growth of the cold neon cluster ion, is small, and dissipated by evaporation of He. It does not cause dissociation of Ne_n^+. Even so, the magic numbers in set 1 are identical to magic numbers reported previously when bare Ne_n were ionized by electrons or photons [41,65], or when HNDs doped with Ne were electron ionized [63,74]. Why? Because multiple collisions between the doped HNDs and He atoms in the evaporation cell will not only completely strip all helium atoms from the doped HND, but also excite the bare Ne_n^+.

Surprisingly, though, we observe a different set of magic numbers, at $n = 7, 13, 19, 26, 34, 55, 71, 81, \ldots$in data set 2 (Figs. 3 and 4), in which the size-to-charge ratio N/z of the HNDs was larger by a factor four, and the charge state may have been as large as $z_{max} = 28$. In Section 4.2 we will compare the observed magic numbers with previous reports, including heavier noble gases, and attempt to correlate them with specific geometric structures. Possible reasons for the change in magic numbers will be discussed in Section 4.3. We begin with an estimate of energetics and cluster temperature in Section 4.1 which will provide useful clues.

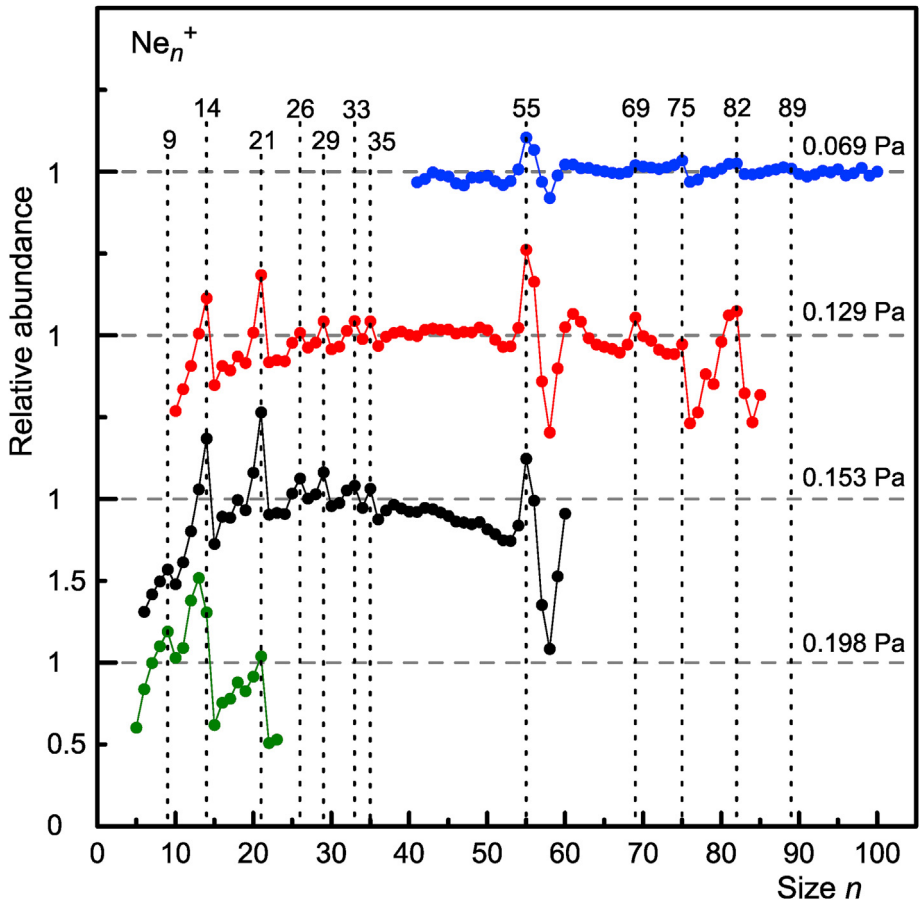

Fig. 2. The relative ion abundance of Ne_n^+ extracted from the four mass spectra in Fig. 1. Magic numbers (defined as those sizes where the ratio I_n/I_{n+1} forms a local maximum) that consistently appear in these and several other measured distributions are marked by vertical lines.

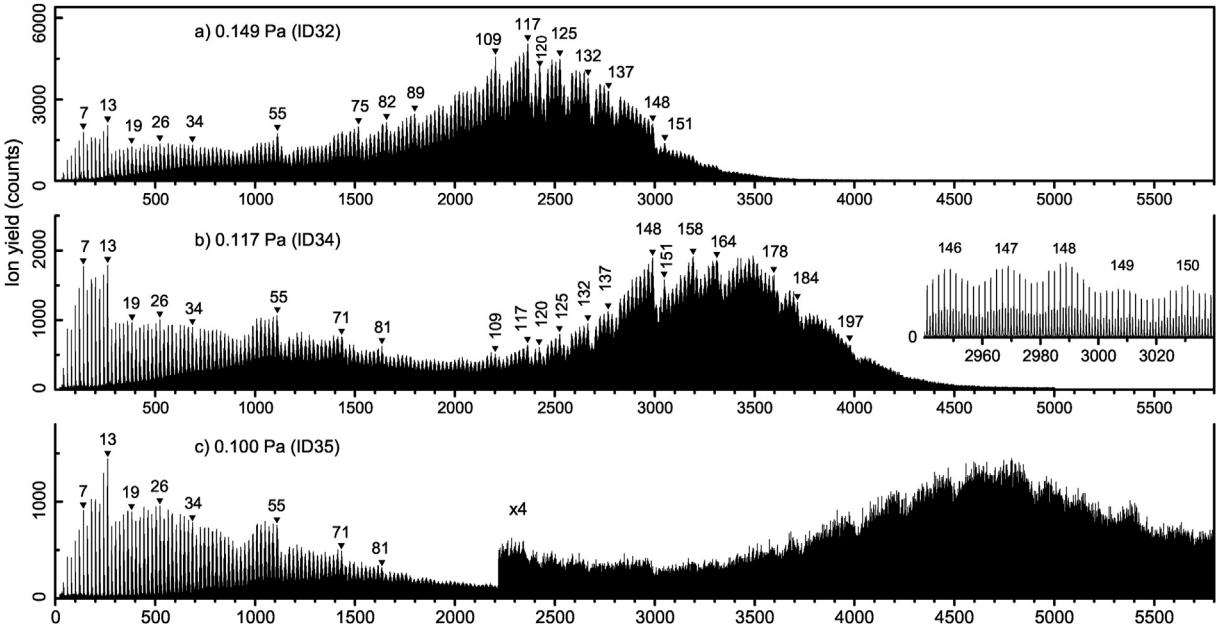

Fig. 3. Three mass spectra of neon clusters grown in large, multiply charged HNDs (data set 2). The pressure P_{He} in the evaporation cell decreases from 0.149 Pa in panel a to 0.100 Pa in panel c. Below $n = 90$ most of the indicated magic numbers (especially in panels b and c) differ from those flagged in Figs. 1 and 2. The inset in panel b reveals the isotopologues of Ne_n^+ around $n \approx 148$.

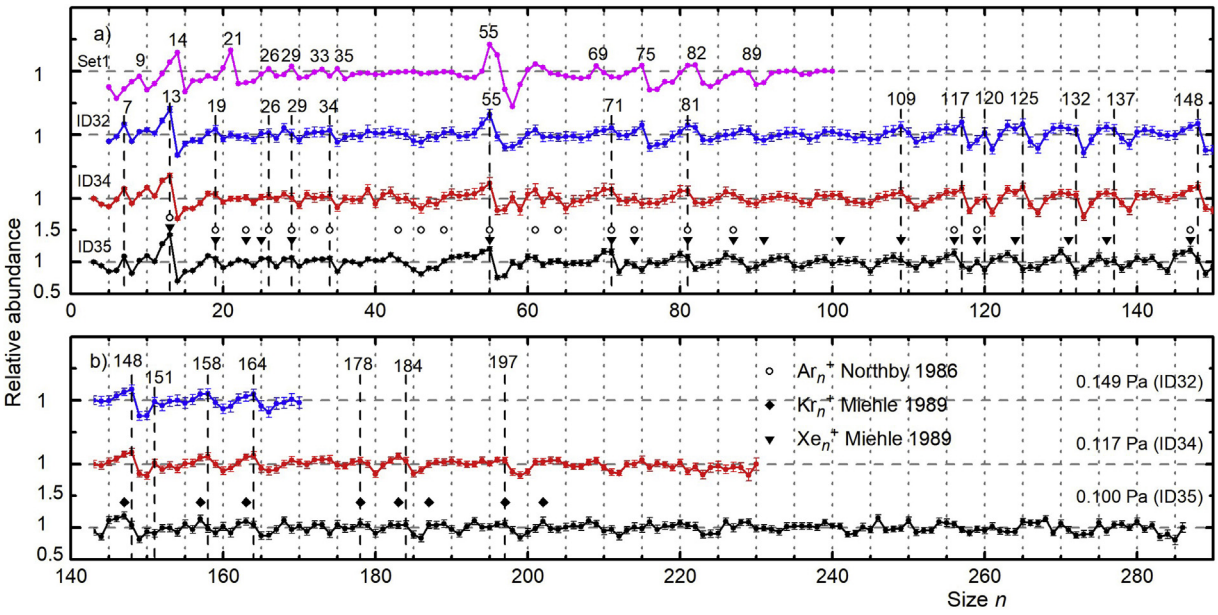

Fig. 4. The top trace in panel a (which covers sizes $n \leq 150$) displays the average relative ion abundance extracted from all spectra in set 1, including the four spectra shown in Figs. 1 and 2. Data in the other traces are extracted from the three mass spectra in Fig. 3 (set 2); vertical lines mark magic numbers in the bottom trace. Symbols above the bottom trace indicate magic numbers reported in the literature for Ar_n^+ [40,57], Kr_n^+, and Xe_n^+ [44].

4.1. Energetics, annealing, melting

In this section we consider the energetics related to evaporation from and collisions with Ne_n^+. The dissociation (or evaporation) energy D_n decreases with size n [75]. Beyond closure of the first solvation shell at $n \approx 13$, the cohesive energy of bulk neon (20 meV) will provide a reasonable estimate. This value will be denoted D_{av}; it presents an average that ignores possible local anomalies in the size dependence of D_n.

In its simplest version, the evaporative model assumes that the vibrational heat capacity of a cluster (or cluster ion) equals the classical (equipartition) value, $C_n = (3n\text{-}6)k_B$. In the following we will neglect the 6 translational and rotational degrees of freedom. However, because of their small atomic mass, low dissociation energy, and correspondingly low vibrational temperature, neon clusters show significant quantum effects [76–78]. We adopt the Debye theory to estimate their heat capacity [79]. According to this model, the heat capacity of elemental solids (with one atom per primitive unit cell) equals

$$C_n = 9nk_B\left(\frac{T}{\theta}\right)^3 \int_0^{\Theta/T} x^4 e^x (e^x - 1)^{-2} dx \qquad (1)$$

The Debye temperature θ of neon in the low-temperature limit equals 74.6 K [80]. The estimated vibrational temperature of medium-sized neon clusters subject to unimolecular dissociation equals $T \approx D_{av}/(\gamma k_B)$ where $\gamma \approx 25$ is the Gspann factor [34]. With $D_{av} \approx 20$ meV we obtain $T \approx 10$ K. In our experiments, the evaporation rate is raised from $k \approx 10^4$ s^{-1} in a typical metastable time window to $k \approx 10^6$ s^{-1} in the evaporation cell [67]. This decreases the Gspann factor by about 30 % [81], hence we estimate $T \approx 13$ K. At that temperature the heat capacity of Ne_n^+, estimated from eq. (1), is reduced with respect to the classical value by a factor 0.29. The reduction is probably even stronger, because the finite size of the cluster eliminates the long-wavelength, low-frequency phonons which contribute most strongly as T approaches zero.

The (vibrational) excitation energy of Ne_n^+ at 13 K is easily obtained by integrating $C_n dT$, with the result $E_n^* \approx 0.29\, n$ meV. This implies that, shortly after their last collision, cluster ions containing fewer than ≈70 atoms will no longer be able to evaporate another atom. In this scenario the relative cluster ion abundance becomes proportional to the relative dissociation energy, defined as D_n divided by the local average of D_n [82–84].

Next, we estimate the energetics of collisions with He in the evaporation cell [67]. Each collision transfers about 58 meV. This will lead to the rapid evaporation of about 94 He atoms from the cold (0.37 K), doped HND without heating the embedded neon cluster ion. Once all He atoms have been stripped, the average temperature of bare Ne_n^+ will rise to about 13 K.

Our discussion so far has ignored possible phase transitions. The melting temperatures of neutral Ne_n have been calculated, with quantum corrections, to be just above 11 K for $n = 13$ and 55, and about 14 K for $n = 147$ [76,85]. From a graph of $C_n(T)$ in Ref. [76] we estimate that the latent heat of melting equals roughly 23 meV for Ne_{13}, 105 meV for Ne_{55}, and 260 meV for Ne_{147}. Thus, except for very small clusters, a single collision will raise the temperature to the melting point, but not fully melt a solid cluster.

Several caveats are in order. First, in an evaporative ensemble clusters are isolated, and the concept of temperature is subtle [86,87]. Second, anomalies in the size dependence of D_n will lead to anomalies in the size dependence of $T(n)$; more stable clusters can accommodate larger excitation energies and will be correspondingly hotter. Third, relatively stable clusters such as the closed-shell icosahedral Ne_{13}, Ne_{55}, and Ne_{147} will feature relatively large melting temperatures and latent heats. Fourth, in the experiment we are dealing with charged clusters, but the computed thermodynamic properties pertain to neutral clusters.

4.2. Magic numbers and atomic structure

We start with a discussion of the measured abundance of small Ne_n^+ ions, containing fewer than 58 atoms, for which dissociation energies have been calculated [7,88]. In Section 4.1 we have argued that the heat capacity of Ne_n^+ at temperatures relevant to the experiment (about 13 K) is very small, hence the relative cluster ion

abundance is expected to closely track the relative dissociation energy. Fig. 5a displays the relative abundance of Ne_n^+ formed in large, multiply charged HNDs at the lowest pressure in the evaporation cell (data from the bottom trace in Fig. 4a). Fig. 5b displays the averaged relative abundance of Ne_n^+ from data set 1 (data from the top trace in Fig. 4a). Calvo et al. have located the stable structures of cationic neon clusters containing up to 57 atoms using a diatomic-in-molecules potential energy surface [7]. The computed relative dissociation energies are displayed in Fig. 5c (absolute values are compiled in Fig. S2 in the Supplemental Material). Fig. 5d represents values corrected for the zero-point energy in the harmonic approximation [7]. Sebastianelli et al. have

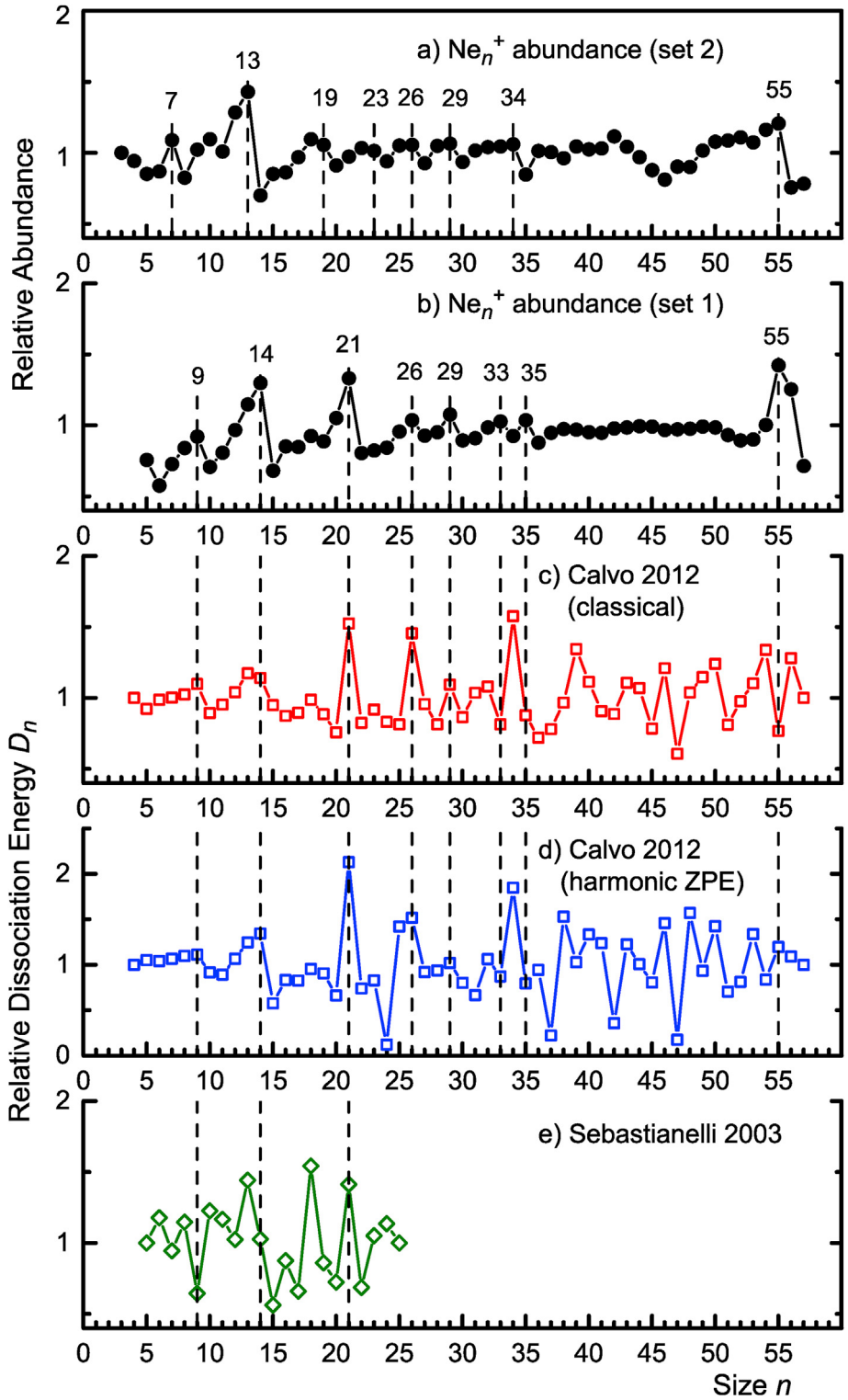

Fig. 5. Panels a and b display relative ion abundances, reproduced from the bottom and top traces of Fig. 4a. Relative dissociation energies calculated by Calvo et al. [7] are displayed in panels c and d; the data in panel d are corrected for the zero-point energy. Energies calculated by Sebastianelli et al. [88] are shown in panel e.

computed D_n for $n \leq 25$ using a simple model in which the sum of the interactions among different size polygons of neon atoms surrounding an ionic dimer core was optimized [88]; relative dissociation energies derived from their work are displayed in Fig. 5e.

Below $n = 30$ the relative abundances in Fig. 5b correlate reasonably well with the relative dissociation energies in Fig. 5d; both sets feature anomalies at $n = 9, 14$ 21, and 26. The agreement is poor for larger sizes, possibly because lowest-energy structures may have been missed in the theoretical work (the search for favorable structures by unbiased basin-hopping global optimization was limited to $n \leq 30$). Although the 56-mer shows no enhancement in the relative dissociation energy, it shares a unique property with the 14-mer and 21-mer: While for most sizes zero-point motion is sufficiently high to blur the picture of a single well-defined structure, the 14-, 21- and 56-mer exhibit a high degree of vibrational localization at their classical minimum energy structure [7].

There is no theoretical work pertaining to larger Ne_n^+, nor for Ar_n^+, Kr_n^+, or Xe_n^+. Instead we will consult studies of neutral noble gas clusters, beginning with simple sphere packing models. Mackay concluded that the most compact, dense cluster sizes have icosahedral (I_h) symmetry, where a central atom is surrounded by K shells of atoms [89]. Each shell has 20 triangular facets. The 12 atoms in the first shell form the vertices of an icosahedron. The number of atoms in the 2nd through 4th shell equals 42, 92, and 162. The total number of atoms in the first four Mackay icosahedra equals 13, 55, 147, 309. Cuboctahedra cut from a fcc crystal would contain the same number of atoms, but they are energetically less favorable because of the low-density (100) arrangement of atoms in their square facets.

For some charged van der Waals clusters, including Xe [44] and CO [90], prominent magic numbers coincide with the anticipated shell closings at 13, 55, 147, 309 even though the delocalization of the charge at the cluster center will break the icosahedral symmetry. For other systems, including Ne, Ar, and Kr, magic numbers expected for the first few icosahedral shell closings are weak, entirely absent, or shifted to 14, 56, 148 [29,41–44]. An ad-hoc explanation of these shifts is the fact that a dimer ion at the cluster center is strongly contracted relative to a neutral dimer. The global minimum structures calculated by Calvo et al. for Ne_{14}^+ and Ne_{56}^+ confirm this explanation [7].

Next, we discuss magic numbers observed between icosahedral shell closings. Except for small clusters, a systematic search for the global minimum structure is not practical, even if a simple pair potential is used to compute the total cluster energy. The problem simplifies if it is assumed that the atoms in the K^{th}, incomplete, outermost shell arrange on top of a rigid Mackay icosahedron with K-1 complete shells [73,91,92]. Even so, the agreement among predicted values, and between prediction and observation, is disappointing.

We will merely sketch some basic ideas for the prediction of subshell closures. For van der Waals bound systems, the relatively strong interaction with nearest neighbors favors growth of a single island. Atoms will completely cover one facet before growing on another one, and growth on adjacent facets is favored over growth on disconnected facets. In very large calcium clusters, a sequence of 20 magic numbers has been observed when going from a K-shell to a K+1-shell Mackay icosahedron, each number indicating the filling of one facet [73].

The number of atoms in each of the facets of a Mackay icosahedron equals 3, 6, 10, 15 for $K = 1$ through 4. Within these facets the atoms are arranged in (approximately) close-packed layers, with a stacking sequence ABCA… between layers, the same as in a face-centered cubic (fcc) crystal. However, the first few atoms added to a Mackay icosahedron are arranged in the stacking sequence ABA. For example, the first atom added to the 13-mer resides atop the central atom. A first major subshell closure is expected when five adjacent facets are covered and topped by one additional atom. The magic numbers are thus predicted at 13 + 5*1 + 1 = 19 (the so-called double icosahedron), 55 + 5*3 + 1 = 71, and 147 + 5*6 + 1 = 178. The first two of these are clearly observed in the bottom trace in Fig. 4a. The third predicted anomaly correlates with an observed anomaly at 179, presumably shifted by one because the cluster core contains 148 rather than 147 atoms.

Covering another three adjacent facets plus adding an apex atom would predict magic numbers at 23, 81, and 197. The first of these predictions does not mesh with the data in Fig. 4 (bottom trace), but the other ones do.

Eventually, as a subshell grows, a complete rearrangement from a stacking sequence ABA to ABC will lower the total energy of the system. The size where this transition occurs is subject to debate, as is the size where the energy of a cuboctahedral cluster with atoms in a crystalline (fcc) arrangement will drop below that of the Mackay icosahedron [93].

One may try to predict magic numbers by considering peeling off atoms from a Mackay icosahedron, but that discussion would be beyond the scope of this manuscript. Instead, we will look for similarities between magic numbers observed in data set 2 (bottom traces in Fig. 4) and previous reports. Symbols plotted above the bottom trace indicate magic numbers reported for Ar_n^+ [40,57], Kr_n^+, and Xe_n^+ [44]. Between $n = 13$ and 34 the agreement between currently and previously observed magic numbers is good. The expected magic numbers at 55, 71, and 81 are clearly present. Between $n = 109$ and 197 the agreement is excellent, especially if we keep in mind that a shift of the magic number from 147 in mass spectra of Kr_n^+ and Xe_n^+ [44] to 148 in the current data accounts for a similar shift in subshell closures. There are very few anomalies indicated between $n = 87$ and 147 in the Ar_n^+ data because the authors chose to flag local minima rather than maxima [40,57]. Most of these minima (observed at $n = 102$, 105, 112, 126, 132, 137, 179, 184, 199, 216, and 232) also appear in our data.

4.3. Magic change of magic numbers

To summarize our observations: First, the magic numbers observed in data set 1 (including 14, 21, 35, 55/56, 75, 82) agree with values previously reported [41,63,65,66] for Ne_n^+. Second, these magic numbers are immune to changes in the collision pressure. Third, the magic numbers observed in data set 2, at lowest collision pressure, are different: 13, 19, 34, 55, 71, 81. Fourth, the numbers in data set 2 agree closely with numbers reported in Ar_n^+, Kr_n^+ and Xe_n^+ spectra [40,44,57]. What causes this change? How is such a change compatible with the alleged correlation between abundance and stability?

We can think of three possible reasons. The first one would be a misassignment of n, caused by impurities. The HNDs used to record data set 2 had a size-to-charge ratio of $N/z = 1.9 \times 10^5$. Their maximum possible charge state is $z_{max} = 28$ which would correspond to $N = 5.3 \times 10^6$. Water is the most prevalent contaminant, which could possibly lead to, for example, $Ne_{12}H_2O^+$ or $Ne_{12}H_3O^+$. These ions may feature high stability but they would appear 2 or 1 u below the magic Ne_{13}^+; their presence is easily ruled out. Likewise, although protonated neon clusters have been reported to feature magic numbers different from those of Ne_n^+ [63], the mass shift by +1 u would be easily detected.

Second, because of the closeness between the estimated cluster temperatures and the calculated melting temperatures one might speculate that the two different sequences of magic numbers pertain to different phases. However, this runs counter to the basic

understanding of clusters in an evaporative ensemble. The temperature (or, better, its vibrational energy distribution) will depend on n, on the dissociation energies and heat capacities of the n-mer and the n+1-mer, and on the time elapsed since formation of the ensemble, but not on the initial conditions (i.e., size distribution or initial excitation energy). Furthermore, magic numbers due to geometric shell closure have been shown to disappear when the cluster temperature is raised above the melting temperature [45,94]. Those experiments involved large neutral sodium clusters, but there is no reason why this should not apply to small Ne_n^+ as well (with perhaps one exception: Closure of the first solvation shell may be accompanied by a substantial drop in D_n, even if the cluster were liquid).

Third, the clusters in data sets 1 and 2 have different histories. Perhaps one data set pertains to fully annealed clusters but the other does not? Neon cluster ions are grown in HNDs by successive capture of atoms. The temperature of large HNDs is 0.37 K; it is likely that the Ne_n^+ embedded in the HND are amorphous. Metal clusters grown in large neutral HNDs have been shown to form wires rather than compact clusters [95]. In a recent publication we have modeled the fate of Ne_n^+ grown in singly charged HNDs [67]. The droplet will capture about 100 Ne atoms in the pickup cell. About 30 collisions are required between the bare Ne_n^+ and He in the evaporation cell in order to produce, say, Ne_{13}^+. Each collision will partly melt the cluster (see Section 4.1). One could hardly think of a better annealing process.

On the other hand, it is difficult to characterize the provenance of Ne_n^+ ions recorded in data set 2. As discussed elsewhere, a size-to-charge selected HND with $z_{max} = 4$ will offer 10 different pathways to produce singly charged neon clusters [67]. With $z_{max} = 28$, a whole zoo of singly charged neon clusters will form. Let us look at one specific precursor, a z-fold charged HND. It will form an incubator for z singly charged neon clusters. As the clusters grow in the pickup cell, the HND will shrink and, upon reaching the Rayleigh limit, eject a singly charged, nearly bare Ne_{n1}^+. The z-1 clusters embedded in the HND will keep growing until the Rayleigh limit is reached once again, and a singly charged, nearly bare Ne_{n2}^+ will be ejected, with $n_2 > n_1$. Cluster growth stops when the doped HND exits the pickup cell, but the ejection of singly charged, nearly bare neon clusters will continue in the evaporation cell until the HND hosts a single neon cluster ion. Which of these z singly charged clusters will populate the mass spectra in Fig. 3? The spectra are approximately bimodal. Statistically speaking, the ejected cluster ions outnumber the lucky one that remains as lone survivor in the HND. At the exit of the evaporation cell, this lone survivor will be larger than any of its former roommates; some of those castaways will not even make it to the exit of the cell. Thus, the likely precursors of the large cluster ions in Fig. 3 are the survivors, while the castaways feed the low mass range, giving rise to magic numbers at $n = 7$ through 55, 71, 81 in Fig. 3b and c. A transition occurs at the highest collision pressure (Fig. 3a), when the large clusters spill into the region of medium sizes, and the magic numbers change to 55/56, 75, 82, 89.

So far, we have argued that the two different sets of magic numbers correlate with different cluster histories. Set A (including 9, 14, 21, 35, 55/56, 75, 82, 89, 109, 117, 125,…) correlates with clusters that were either formed in singly charged HND (see top trace in Fig. 4a), or that remained as sole survivors in HNDs until their z-1 competitors were ejected. Set B (7, 13, 19, 34, 55, 71, 81) is the fingerprint of nearly bare Ne_n^+ ejected from multiply charged HNDs.

But if magic numbers reflect cluster stability, then two different sets of magic numbers imply that there are two distinct structural families. Experimental and theoretical work pertaining to Ar_n^+ and Xe_n^+ does, indeed, suggest that two families of isomers coexist [96,97]. The families differ in the nature of the ionic core, either a linear trimer or a linear tetramer; perpendicular isomers of Ar_3^+ have been reported as well [12]. The isomers do not interconvert at low temperature [97].

The properties of Ne_2^+, Ne_3^+, and Ne_4^+ have been explored in several theoretical studies [6,98–101]. Ne_3^+ is a very floppy molecule [98] which would rule out the existence of distinct isomers that do not convert at our experimental conditions. But the structural families that seem to exist for argon and xenon cluster ions differ by the size of the ionic core, not its structure. Either way, it is conceivable that the barrier between the two alleged isomers increases when neutral atoms are bound to the ionic core. In Section 4.1 we have argued that the energy transferred to Ne_n^+ in collisions with He will suffice to raise the cluster temperature to the melting point, but not to fully melt the cluster. As long as the cluster core remains frozen, the outer, molten shells would return to their previous structures as the cluster cools down again.

Questions remain. We have no compelling explanation why a specific history (e.g., ejection from a multiply charged HND) correlates with one specific structural family (characterized by magic numbers in set B). In the past, magic numbers were usually found to be highly reproducible, but there is one striking counterexample: Mass spectra of argon cluster ions, produced by electron, photon or Penning ionization of neutral precursors, either bare or embedded in helium, are characterized by a deep local minimum at $n = 20$, but no enhanced signal at $n = 13$ [29,42,44,51,54–56,58–60]. If, however, Ar_n^+ are formed by nucleation and growth on argon ions formed in a corona discharge, one observes a maximum at $n = 13$ and 19 but no minimum at 20 [40]. Several other differences have been reported for larger sizes [102].

A better understanding of factors that lead to two different sets of magic numbers requires further work. On the experimental side, two approaches appear promising: First, mass-selected Ne_n^+ could be collided with He or other atoms in a separate collision cell. What are the preferred fragment ions if the collision energy is varied? Does it matter if the precursor ion Ne_n^+ is taken from the ensemble of clusters emerged via history 1, or history 2? Second, and more promising, would be spectroscopic work. Isomeric structures in argon and xenon cluster have been revealed by photoabsorption and photodissociation [9,11,103]. The estimated absorption spectrum of Ne_3^+ has been calculated to peak at about 470 nm [104]; absorption in this range would lead to the loss of several Ne atoms and be readily detectable.

5. Conclusion

The present work extends the size range for which abundance anomalies are observed in mass spectra of neon clusters from $n <$ 90 to $n \approx 200$. The numbers observed in this extended range agree well with data in some previous reports for heavier noble gases. Below $n \approx 100$, though, we observe two different sets of magic numbers, depending on the experimental conditions. One set fully agrees with magic numbers previously reported for Ne_n^+; it is observed if neon cluster ions are grown in singly charged HNDs. The other set is traced to Ne_n^+ that have been ejected from multiply charged HNDs. The observations point to the existence of structural isomers that do not interconvert. Experiments that could possibly confirm this hypothesis have been proposed.

Declaration of competing interest

The authors declare that they have no known competing financial interests or personal relationships that could have appeared to influence the work reported in this paper.

Acknowledgement

We thank F. Calvo for providing the data published in Fig. 1 of Ref. [7]. This work was supported by the Austrian Science Fund, FWF (Projects I4130, P31149, T1181, and W1259).

Appendix A. Supplementary data

Supplementary data to this article can be found online at https://doi.org/10.1016/j.ijms.2021.116528.

References

[1] D.J. Wales, M.A. Miller, T.R. Walsh, Archetypal energy landscapes, Nature 394 (1998) 758–760.
[2] M.R. Hoare, J.A. McInnes, Morphology and statistical statics of simple microclusters, Adv. Phys. 32 (1983) 791–821.
[3] E.E. Polymeropoulos, J. Brickmann, On the origin of the occurrence of magic numbers in cluster size distributions of xenon in the compressed gas-phase, Chem. Phys. Lett. 96 (1983) 273–275.
[4] P. Paska, D. Hrivák, R. Kalus, Diatomics-in-molecules study of the geometric and electronic structure of Xe_n^+ clusters, Chem. Phys. 286 (2003) 237–248.
[5] M. Slama, K. Issa, F.E. Ben Mohamed, M.B. Rhouma, F. Spiegelman, Structure and stability of Na^+Xe_n clusters, Eur. Phys. J. D 70 (2016) 242.
[6] F.A. Gianturco, F. Sebastianelli, Computed structures and energetics of ionic neon clusters using DFT correlation corrections, Eur. Phys. J. D 10 (2000) 399–414.
[7] F. Calvo, F.Y. Naumkin, D.J. Wales, Nuclear quantum effects on the stability of cationic neon clusters, Chem. Phys. Lett. 551 (2012) 38–41.
[8] J. Urban, P. Mach, J. Mášik, I. Hubac, V. Staemmler, Ground and excited states of the Ne_3^+ molecule, Chem. Phys. 255 (2000) 15–22.
[9] H. Haberland, B. von Issendorff, T. Kolar, C. Ludewigt, A. Risch, Electronic and geometric structure of Ar_n^+ and Xe_n^+ clusters: the solvation of rare-gas ions by their parent atoms, Phys. Rev. Lett. 67 (1991) 3290–3293.
[10] T. Laarmann, A. Kanaev, K. von Haeften, H. Wabnitz, R.v. Pietrowski, T. Möller, Evolution of the charge localization process in xenon cluster ions: from tetramer to dimer cores as a function of cluster size, J. Chem. Phys. 116 (2002) 7558.
[11] B. von Issendorff, A. Hofmann, H. Haberland, Observation of linear isomers of the ionized rare gas tetramers Ar_4^+ and Xe_4^+, J. Chem. Phys. 111 (1999) 2513–2518.
[12] R. Kalus, M. Stachon, F.X. Gadea, On the competition between linear and perpendicular isomers in photodynamics of cationic argon trimers, J. Chem. Phys. 137 (2012) 234308.
[13] M. Fieber, A.M.G. Ding, P.J. Kuntz, A diatomics-in-molecules model for singly ionized neon clusters, Z. Phys. D 23 (1992) 171–179.
[14] A. Volk, P. Thaler, D. Knez, A.W. Hauser, J. Steurer, W. Grogger, F. Hofer, W.E. Ernst, The impact of doping rates on the morphologies of silver and gold nanowires grown in helium nanodroplets, Phys. Chem. Chem. Phys. 18 (2016) 1451–1459.
[15] J. Farges, M.F. Deferaudy, B. Raoult, G. Torchet, Noncrystalline structure of argon clusters. II. Multilayer icosahedral structure of Ar_N clusters $50<N<750$, J. Chem. Phys. 84 (1986) 3491–3501.
[16] B.W. van de Waal, G. Torchet, M.F. de Feraudy, Structure of large argon clusters Ar_N, $10^3 < N < 10^5$: experiments and simulations, Chem. Phys. Lett. 331 (2000) 57–63.
[17] D. Schooss, M.N. Blom, J.H. Parks, B. von Issendorff, H. Haberland, M.M. Kappes, The Structures of Ag_{55}^+ and Ag_{55}: trapped ion electron diffraction and density functional theory, Nano Lett. 5 (2005) 1972–1977.
[18] A.P. Woodham, A. Fielicke, Gold clusters in the gas phase, in: D.M.P. Mingos (Ed.), Gold Clusters, Colloids and Nanoparticles I, 2014, pp. 243–278.
[19] G.E. Douberly, R.E. Miller, S.S. Xantheas, Formation of exotic networks of water clusters in helium droplets facilitated by the presence of neon atoms, J. Am. Chem. Soc. 139 (2017) 4152–4156.
[20] H.J. Zeng, N. Yang, M.A. Johnson, Introductory lecture: advances in ion spectroscopy: from astrophysics to biology, Faraday Discuss 217 (2019) 8–33.
[21] A. Kaiser, J. Postler, M. Ončák, M. Kuhn, M. Renzler, S. Spieler, M. Simpson, M. Gatchell, M.K. Beyer, R. Wester, F.A. Gianturco, P. Scheier, F. Calvo, E. Yurtsever, Isomeric Broadening of C_{60}^+ electronic excitation in helium droplets: experiments meet theory, J. Phys. Chem. Lett. 9 (2018) 1237–1242.
[22] L. Kranabetter, N.K. Bersenkowitsch, P. Martini, M. Gatchell, M. Kuhn, F. Laimer, A. Schiller, M.K. Beyer, M. Ončák, P. Scheier, Considerable matrix shift in the electronic transitions of helium-solvated cesium dimer cation $Cs_2He_n^+$, Phys. Chem. Chem. Phys. 21 (2019) 25362–25368.
[23] S. Albertini, P. Martini, A. Schiller, H. Schöbel, E. Ghavidel, M. Ončák, O. Echt, P. Scheier, Electronic transitions in Rb_2^+ dimers solvated in helium, Theor. Chem. Acc. (2021) submitted.
[24] C.E. Klots, The evaporative ensemble, Z. Phys. D 5 (1987) 83–89.
[25] C.E. Klots, Kinetic methods for quantifying magic, Z. Phys. D 21 (1991) 335–342.
[26] K. Hansen, From abundance spectra to cluster energies, Surf. Rev. Lett. 3 (1996) 597–600.
[27] K. Hansen, U. Näher, Evaporation and cluster abundance spectra, Phys. Rev., A 60 (1999) 1240–1250.
[28] C.E. Klots, Evaporation from small particles, J. Phys. Chem. 92 (1988) 5864–5868.
[29] S. Prasalovich, K. Hansen, M. Kjellberg, V.N. Popok, E.E.B. Campbell, Surface entropy of rare-gas clusters, J. Chem. Phys. 123 (2005), 084317.
[30] O. Echt, D. Kreisle, M. Knapp, E. Recknagel, Evolution of magic numbers in mass spectra of water clusters, Chem. Phys. Lett. 108 (1984) 401–407.
[31] J.M. Soler, J.J. Saenz, N. Garcia, O. Echt, The effect of ionization on magic numbers of rare-gas clusters, Chem. Phys. Lett. 109 (1984) 71–75.
[32] D. Kreisle, O. Echt, M. Knapp, E. Recknagel, Time-dependent size distribution of xenon-cluster ions, Phys. Rev., A 33 (1986) 768.
[33] T.D. Märk, P. Scheier, Experimental evidence for the time dependence of the metastable decay rate of Ne cluster ions: a further key to the magic number problem, J. Chem. Phys. 87 (1987) 1456–1458.
[34] C.E. Klots, Temperature of evaporating clusters, Nature 327 (1987) 222–223.
[35] R. Casero, J.M. Soler, Onset and evolution of "magic numbers" in mass spectra of molecular clusters, J. Chem. Phys. 95 (1991) 2927–2935.
[36] O. Echt, P.D. Dao, S. Morgan, A.W. Castleman, Multiphoton ionization of ammonia clusters and the dissociation dynamics of protonated cluster ions, J. Chem. Phys. 82 (1985) 4076–4085.
[37] O. Echt, M.C. Cook, A.W. Castleman, Multiphoton ionization studies of xenon clusters, Chem. Phys. Lett. 135 (1987) 229–235.
[38] K. Hansen, R. Müller, H. Hohmann, E.E.B. Campbell, Stability of clusters of fullerenes, Z. Phys. D 40 (1997) 361–364.
[39] O. Echt, K. Sattler, E. Recknagel, Magic numbers for sphere packings: experimental verification in free xenon clusters, Phys. Rev. Lett. 47 (1981) 1121–1124.
[40] I.A. Harris, R.S. Kidwell, J.A. Northby, Structure of charged argon clusters formed in a free jet expansion, Phys. Rev. Lett. 53 (1984) 2390–2393.
[41] T.D. Märk, P. Scheier, Production and stability of neon cluster ions up to Ne_{90}^+, Chem. Phys. Lett. 137 (1987) 245–249.
[42] P.G. Lethbridge, A.J. Stace, Reactivity-structure correlations in ion clusters - a study of the unimolecular fragmentation patterns of argon ion clusters, Ar_n^+, for n in the range 30-200, J. Chem. Phys. 89 (1988) 4062–4073.
[43] P.G. Lethbridge, A.J. Stace, An Investigation of the properties of large krypton cluster ions (development of the $P = 3$ and $P = 4$ Mackay icosahedral shells), J. Chem. Phys. 91 (1989) 7685–7692.
[44] W. Miehle, O. Kandler, T. Leisner, O. Echt, Mass spectrometric evidence for icosahedral structure in large rare gas clusters: Ar, Kr, Xe, J. Chem. Phys. 91 (1989) 5940–5952.
[45] T.P. Martin, Shells of atoms, Phys. Rep. 273 (1996) 199–241.
[46] J.E. Campana, T.M. Barlak, R.J. Colton, J.J. Decorpo, J.R. Wyatt, B.I. Dunlap, Effect of cluster surface energies on secondary-ion intensity distributions from ionic crystals, Phys. Rev. Lett. 47 (1981) 1046–1049.
[47] T.P. Martin, Alkali halide clusters and microcrystals, Phys. Rep. 95 (1983) 167–199.
[48] H.W. Kroto, J.R. Heath, S.C. O'Brien, R.F. Curl, R.E. Smalley, C_{60}: buckminsterfullerene, Nature 318 (1985) 162–163.
[49] For some systems (e.g., free-electron like metals) the electronic structure has a larger impact on stability than geometric structure.
[50] M. Brack, The physics of simple metal-clusters - self-consistent jellium model and semiclassical approaches, Rev. Mod. Phys. 65 (1993) 677–732.
[51] T.A. Milne, F.T. Greene, Mass spectrometric observations of argon clusters in nozzle beams. I. General behavior and equilibrium dimer concentrations, J. Chem. Phys. 47 (1967) 4095–4101.
[52] O. Echt, A.R. Flotte, M. Knapp, K. Sattler, E. Recknagel, Magic numbers in mass spectra of Xe, $C_2F_4Cl_2$ and SF_6 clusters, Ber. Bunsenges. Phys. Chem. 86 (1982) 860–865.
[53] M.R. Hoare, Structure and dynamics of simple microclusters, Adv. Chem. Phys. 40 (1979) 49.
[54] A. Ding, J. Hesslich, The abundance of Ar and Kr microclusters generated by supersonic expansion, Chem. Phys. Lett. 94 (1983) 54–57.
[55] H.P. Birkhofer, H. Haberland, M. Winterer, D.R. Worsnop, Penning, photo and electron impact ionization of argon clusters, Ber. Bunsenges. Phys. Chem. 88 (1984) 207–211.
[56] D.R. Worsnop, S.J. Buelow, D.R. Herschbach, Electron bombardment ionization and fragmentation of van der Waals clusters, J. Phys. Chem. 88 (1984) 4506–4509.
[57] I.A. Harris, K.A. Norman, R.V. Mulkern, J.A. Northby, Icosahedral structure of large charged argon clusters, Chem. Phys. Lett. 130 (1986) 316–320.
[58] P. Scheier, T.D. Märk, Mass-resolved argon cluster spectra up to 12000 u (Ar_{300}^+), Int. J. Mass Spectrom. Ion Process. 76 (1987) R11–R15.
[59] F. Ferreira da Silva, P. Bartl, S. Denifl, O. Echt, T.D. Märk, P. Scheier, Argon clusters embedded in helium nanodroplets, Phys. Chem. Chem. Phys. 11 (2009) 9791–9797.
[60] M. Gatchell, P. Martini, L. Kranabetter, B. Rasul, P. Scheier, Magic sizes of cationic and protonated argon clusters, Phys. Rev., A 98 (2018), 022519.
[61] M. Lezius, P. Scheier, A. Stamatovic, T.D. Märk, Production and properties of singly and multiply charged Kr clusters, J. Chem. Phys. 91 (1989) 3240–3245.
[62] H. Schöbel, P. Bartl, C. Leidlmair, S. Denifl, O. Echt, T.D. Märk, P. Scheier, High-resolution mass spectrometric study of pure helium droplets, and droplets doped with krypton, Eur. Phys. J. D 63 (2011) 209–214.

[63] M. Gatchell, P. Martini, A. Schiller, P. Scheier, Protonated clusters of neon and krypton, J. Am. Soc. Mass Spectrom. 30 (2019) 2632–2636.
[64] S. Wei, Z. Shi, A.W. Castleman, Elucidating the origin of magic numbers: trends in the relative binding energies of xenon cluster ions and their implications, J. Chem. Phys. 94 (1991) 8604–8607.
[65] M. Fieber, G. Bröker, A. Ding, The photoionization dynamics of Ne clusters, Z. Phys. D 20 (1991) 21–23.
[66] I. Mähr, F. Zappa, S. Denifl, D. Kubala, O. Echt, T.D. Märk, P. Scheier, Multiply charged neon clusters: failure of the liquid drop model? Phys. Rev. Lett. 98 (2007), 023401.
[67] L. Tiefenthaler, S. Kollotzek, M. Gatchell, K. Hansen, P. Scheier, O. Echt, Isotope enrichment in neon clusters grown in helium nanodroplets, J. Chem. Phys. 153 (2020) 164305.
[68] F. Laimer, L. Kranabetter, L. Tiefenthaler, S. Albertini, F. Zappa, A.M. Ellis, M. Gatchell, P. Scheier, Highly charged droplets of superfluid helium, Phys. Rev. Lett. 123 (2019) 165301.
[69] L. Rayleigh, On the equilibrium of liquid conducting masses charged with electricity, Phil. Mag. 14 (1882) 184–186.
[70] In a Recent Paper We Have Modeled These Events for Doped HNDs with N/z = 7.5×10^4 Whose Maximum Charge Equals Zmax = 4 [67].
[71] S. Ralser, J. Postler, M. Harnisch, A.M. Ellis, P. Scheier, Extracting cluster distributions from mass spectra: IsotopeFit, Int. J. Mass Spectrom. 379 (2015) 194–199.
[72] S. Bjørnholm, J. Borggreen, O. Echt, K. Hansen, J. Pedersen, H.D. Rasmussen, The influence of shells, electron thermodynamics, and evaporation on the abundance spectra of large sodium metal clusters, Z. Phys. D 19 (1991) 47–50.
[73] T.P. Martin, U. Näher, T. Bergmann, H. Göhlich, T. Lange, Observation of icosahedral shells and subshells in calcium clusters, Chem. Phys. Lett. 183 (1991) 119–124.
[74] The Agreement Is Perhaps Not Quite as Striking in the Region above N = 29 Which Is Covered by Only One Previous Report [41]. The Anomalies at N = 33, 35, 55/56, 75, and 82 Are Clearly Visible in that Spectrum but Those at N = 69 and 89 Are Not.
[75] K. Hiraoka, T. Mori, Stability of rare gas cluster ions, J. Chem. Phys. 92 (1990) 4408–4416.
[76] E. Pahl, F. Calvo, L. Koci, P. Schwerdtfeger, Accurate melting temperatures for neon and argon from ab initio Monte Carlo simulations, Angew. Chem. Int. Ed. 47 (2008) 8207–8210.
[77] S. Acosta-Gutierrez, J. Breton, J.M.G. Llorente, J. Hernandez-Rojas, Optimal covering of C_{60} fullerene by rare gases, J. Chem. Phys. 137 (2012), 074306.
[78] F. Calvo, Does vibrational delocalization stabilize multiply-charged neon clusters? J. Phys. Chem. Lett. 1 (2010) 2637–2641.
[79] C. Kittel, Introduction to Solid State Physics, eighth ed., John Wiley & Sons, New York, 2004.
[80] G.R. Stewart, Measurement of low-temperature specific heat, Rev. Sci. Instrum. 54 (1983) 1–11.
[81] K. Hansen, E.E.B. Campbell, Do we know the value of the Gspann parameter? Int. J. Mass Spectrom. 233 (2004) 215–221.
[82] C. Leidlmair, Y. Wang, P. Bartl, H. Schöbel, S. Denifl, M. Probst, M. Alcamí, F. Martín, H. Zettergren, K. Hansen, O. Echt, P. Scheier, Structures, energetics and dynamics of helium adsorbed on isolated fullerene ions, Phys. Rev. Lett. 108 (2012), 076101.
[83] L. An der Lan, P. Bartl, C. Leidlmair, R. Jochum, S. Denifl, O. Echt, P. Scheier, Solvation of Na^+, K^+ and their dimers in helium, Chem. Eur J. 18 (2012) 4411–4418.
[84] T. Gonzalez-Lezana, O. Echt, M. Gatchell, M. Bartolomei, J. Campos-Martinez, P. Scheier, Solvation of ions in helium, Int. Rev. Phys. Chem. 39 (2020) 465–516.
[85] The Bulk Melting Point of Ne Is 24.56 K.
[86] J.U. Andersen, E. Bonderup, K. Hansen, P. Hvelplund, B. Liu, U.V. Pedersen, S. Tomita, Temperature concepts for small, isolated systems; 1/t decay and radiative cooling, Eur. Phys. J. D 24 (2003) 191–196.
[87] K. Hansen, Statistical physics of nanoparticles in the gas phase, in: Springer Series On Atomic, Optical, and Plasma Physics, second ed., vol. 73, Springer, Dordrecht, 2018.
[88] F. Sebastianelli, F.A. Gianturco, E. Yurtsever, Finding the global minima of $(Ne)_n^+$ clusters with non-empirical models: a comparison of results, Chem. Phys. 290 (2003) 279–295.
[89] A.L. Mackay, A dense non-crystalline crystallographic packing of equal spheres, Acta Crystallogr. 15 (1962) 916–918.
[90] O. Kandler, T. Leisner, O. Echt, E. Recknagel, Carbon-monoxide clusters - critical size and magic numbers, Z. Phys. D 10 (1988) 295–301.
[91] J.A. Northby, Structure and binding of lennard-jones clusters: $13 \leq N \leq 147$, J. Chem. Phys. 87 (1987) 6166–6177.
[92] P.G. Lethbridge, G. Del Mistro, A.J. Stace, Hard-sphere cluster-ion structures, J. Chem. Phys. 93 (1990) 1995–2001.
[93] B.W. van de Waal, No evidence for size-dependent icosahedral → fcc structural transition in rare-gas clusters, Phys. Rev. Lett. 76 (1996) 1083–1086.
[94] T.P. Martin, U. Näher, H. Schaber, U. Zimmermann, Evidence for a size-dependent melting of sodium clusters, J. Chem. Phys. 100 (1994) 2322–2324.
[95] M. Schnedlitz, M. Lasserus, D. Knez, A.W. Hauser, F. Hofer, W.E. Ernst, Thermally induced breakup of metallic nanowires: experiment and theory, Phys. Chem. Chem. Phys. 19 (2017) 9402–9408.
[96] D. Hrivnak, R. Kalus, Intra-cluster transitions in small Ar_n^+ cations, Chem. Phys. 264 (2001) 319–331.
[97] J.A. Gascón, R.W. Hall, C. Ludewigt, H. Haberland, Structure of Xe_N^+ clusters ($N = 3$–30): simulation and experiment, J. Chem. Phys. 117 (2002) 8391–8403.
[98] H. Hogreve, The ground-state geometry of the Ne_3^+ trimer, Chem. Phys. Lett. 215 (1993) 72–80.
[99] F.Y. Naumkin, D.J. Wales, Structure and properties of Ne_n^+ clusters from a diatomics-in-molecules approach, Mol. Phys. 93 (1998) 633–648.
[100] X.Y. Sun, Z.R. Li, D. Wu, C.C. Sun, S. Gudowski, F.M. Tao, K.C. Janda, Asymmetrical linear structures including three-electron hemibonds or other interactions in the (*ABA*)-type triatomic cations: Ne_3^+, $(He\text{-}Ne\text{-}He)^+$, $(Ar\text{-}Ne\text{-}Ar)^+$, $(Ar\text{-}O\text{-}Ar)^+$, $(He\text{-}O\text{-}He)^+$, and $(Ar\text{-}He\text{-}Ar)^+$, J. Chem. Phys. 123 (2005) 134304.
[101] E. Yurtsever, F. Sebastianelli, F.A. Gianturco, Fragmentation dynamics of Ne_3^+ clusters: a classical trajectory study, Comput. Mater. Sci. 35 (2006) 163–168.
[102] An alternative explanation for the differences between the magic numbers observed for Ar_n^+ have been suggested by some of us [60]: Anomalies reported by Harris et al. [40] might be due Ar_nH^+ rather than pure Ar_n^+.
[103] M.J. DeLuca, M.A. Johnson, Observation of a UV absorption band in the argon triatomic monopositive ion near 300 nm, Chem. Phys. Lett. 162 (1989) 445–448.
[104] F.Y. Naumkin, Transition intensities in rare gas triatomic ions: DIM versus point-charge approximation, Chem. Phys. 252 (2000) 301–314.